AIAA SciTech Forum
9 - 13 January 2017, Grapevine, Texas
55th AIAA Aerospace Sciences Meeting

Pressure Rate of Strain, Pressure Diffusion and Velocity Pressure Gradient Tensor Measurements in a Cavity Shear Layer Flow

Xiaofeng Liu [1]
San Diego State University, San Diego, California, 92182-1308

and

Joseph Katz [2]
Johns Hopkins University, Baltimore, Maryland, 21218

Pressure related turbulence statistics of a 2D open cavity shear layer flow was investigated experimentally in a water tunnel at a Reynolds number of 40,000. Time-resolved PIV sampled at 4500 frames per second and a field of view of 25×25 mm was used to simultaneously measure the instantaneous velocity, material acceleration and pressure distributions. The pressure was obtained by spatially integrating the measured material acceleration. Results based on 80,000 measurement samples enable direct estimates of components of the pressure-rate-of-strain, pressure diffusion and velocity-pressure-gradient tensors. The pressure and streamwise velocity correlation changes its sign from negative values far upstream from the downstream corner to positive values near the corner due to the strong adverse pressure gradient imposed by the corner. The pressure diffusion term is of the same order as the turbulence production rate, and its distribution pattern is different from the turbulence diffusion. In the shear layer, the streamwise pressure-rate-of-strain term, R_{11}, is mostly negative while the perpendicular term, R_{22}, is positive but with a smaller magnitude, implying turbulent energy redistribution from streamwise to lateral directions. This intermodal fluctuation energy transfer pattern is reversed on top of the trailing corner of the cavity, indicating the complexity of the pressure-related turbulence transport terms associated with the cavity shear layer flow, especially around the corner area.

Nomenclature

C_p	=	pressure coefficient
d	=	displacement of seeding particles within the PIV interrogation window
L	=	cavity length
u	=	streamwise velocity component in the x-direction
v	=	lateral velocity component in the y-direction
$\overline{u}$	=	time-averaged streamwise velocity component
$\overline{v}$	=	time-averaged lateral velocity component
u'	=	fluctuating streamwise velocity component
v'	=	fluctuating lateral velocity component
U_e	=	external freestream velocity
$\vec{x}_a$	=	location of particle group within the PIV interrogation window
δt	=	time interval between consecutive PIV images
θ	=	momentum thickness

[1] Assistant Professor, Department of Aerospace Engineering, SDSU. AIAA Associate Fellow.
Email: Xiaofeng.Liu@mail.sdsu.edu.
[2] Professor, Department of Mechanical Engineering, Johns Hopkins University. AIAA Senior Member.

I. Introduction

TURBULENCE is a fundamental flow phenomenon widely seen in nature and engineering applications. To accurately quantify the effects caused by turbulence, adequate physics-based turbulence modeling is needed. This is of pivotal importance to CFD in particular and the simulation-based engineering science (SBES) in general. Example application areas[1] (Oden *et al.*, 2006, NSF blue ribbon panel report) that would be affected by physics-based turbulence modeling include, but not limited to, aerodynamic force prediction for aircraft, automobile, ship propeller, wind turbine, and jet engine designs, hazardous weather forecasting, oceanic flow influence on global climate changes, evaluation of cardiovascular flow on human heart health, etc.

Consistent with the NSF report, a NASA report[2] *CFD Vision 2030 Study: A Path to Revolutionary Computational Aerosciences* (Slotnick *et al.*, 2014) places exclusive emphasis on both RANS (Reynolds-Averaged Navier-Stokes) and LES (Large Eddy Simulation) approaches as the choice of methods for computational tools to cope with grand challenges envisioned by 2030. A critical element to the process of achieving physics-based predictive modeling is high-quality experimental data at realistic high Reynolds numbers. However, lack of data, especially the experimentally obtained pressure-related terms, e.g., pressure diffusion and pressure strain terms in the Reynolds stress transport equation, has greatly hindered the development of physics-based turbulence models. As noted by the NASA CFD Vision 2030 report, RANS turbulence models have nearly seen stagnant development for 20 years[2-3] (Slotnick *et al.*, 2014; Wilcox, 2006). It is based on this observation that this paper attempts to present some recently obtained experimental data on the pressure-related statistical terms for a shear layer flow over an open cavity.

Major difficulties that result in the prolonged lack of experimental data on pressure-related turbulence statistics reside in the lack of reliable means for simultaneous measurement of instantaneous pressure and velocity distributions in flow field. In the past decade or so, efforts in developing non-intrusive pressure measurement techniques have been carried out extensively in the fluids community. It is shown that the instantaneous pressure distribution in an incompressible turbulent flow field can be reconstructed by integration of the measured material acceleration, as demonstrated by Liu and Katz[4-7] (2003, 2006, 2008, 2013), van Oudheusden[8] (2008), Ragni *et al.*[9] (2009) and Joshi *et al.*[10] (2014), to name a few. The material acceleration constitutes the dominant contributor to pressure gradient with the viscous term being negligible for flow at high Reynolds number and away from wall, and can be measured non-intrusively using PIV (Particle Image Velocimetry), either discretely[4-7] or continuously[7,10] time-resolved. Once the material acceleration is obtained, the pressure gradient is known. Further integrating it will obtain the pressure. So far there are three major types of integration methods, i.e., *direct line integration*, *Poisson equation* and *least-square reconstruction* that have been introduced and developed for pressure reconstruction from the measured material acceleration. For direct line integration, representative method is the so-called *Circular Virtual Boundary, Omni-Directional Integration*[4-7] over the entire measurement domain, which was evolved recently to a new algorithm featuring *rotating parallel ray*[11] as integration path guidance. Representative *Poisson equation* approach can be found in de Kat and van Oudheusden[12-13] (2010, 2012), Violato *et al.*[14] (2011), and Auteri *et al.*[15] (2015), etc. Review and comparison of the *direct line integration* and *Poisson equation* pressure reconstruction approaches can be found in Charonko *et al.*[16] (2010), and van Oudheusden[17] (2013). The robustness of the omni-directional integration method has been confirmed by Charonko *et al.*[16] (2010). The *least-square reconstruction* approach[18] (Jeon *et al.*, 2015) was recently used to experimentally obtain instantaneous pressure field in a wake of a separated flow over an airfoil. This approach was also referred to as *direct matrix inversion* by Liu and Katz[5] (2006).

The aforementioned efforts in PIV-based pressure measurement tool development provide the possibility of measuring much-needed pressure-related statistics in turbulent flows. In particular, this paper reports the results of the planar pressure diffusion and pressure-strain terms measured in a cavity shear layer flow at a Reynolds number of 40,000 based on the cavity length. Some of these results were presented orally in APS DFD meetings[19-21] in 2007, 2008 and 2014, respectively.

We need to recognize that prior to the results presented in this paper, there have been attempts to measure the planar pressure diffusion and/or pressure-strain terms either directly or indirectly before. For example, Kawata and Obi[22] (2014) measured pressure-related statistics for a calendar wake flow at a cylinder diameter-based Reynolds number of 7,800 by reconstructing the POD modes of pressure with a 2-D Poisson equation. Liu and Thomas[23] (2004), Gutmark and Wygnanski[24] (1976) and Wygnanski and Fiedler[25] (1969) obtained pressure diffusion estimates by balancing all other terms in turbulence kinetic energy transport equation. As for point pressure-velocity correlation measurement, representative efforts using combination of pressure and X-wire probes include Kawata *et al.*[26] (2014) in a near wake flow, Terashima *et al.*[27] (2012) in a planar jet, Naka and Obi[28] (2009) in free shear flows, and Naka *et al.* [29] (2006) in a mixing layer. It is worth mentioning that as an earlier effort using a four-hole cobra

probe, Hooper and Musgrove[30] (1997) conducted point pressure-velocity correlation measurement in a turbulent pipe flow.

The organization of this paper is as follows. Section II presents the experimental setup. Section III reviews briefly the material acceleration and the non-intrusive pressure measurement techniques used in the experiment. The measurement results are shown in Section IV, which is followed by discussion and conclusion in Section V.

II. Experimental Setup

The experiment has been conducted in a small water tunnel described in Gopalan and Katz[31] (2000) and Liu and Katz[5] (2006). Details about the experimental setup can be found in Liu and Katz[7] (2013). To present the new information on the pressure-related statistics, only essential features about the setup are repeated here. As sketched in Figure 1, a 38.1 mm long, 50.8 mm wide and 30.0 mm deep two-dimensional cavity model is constructed of a transparent acrylic insert that is installed in the 50.8 mm × 63.5 mm test section. A 13 mm long region with tripping grooves, each with a notch depth of 0.46 mm and width of 1.00 mm, is machined at the beginning of the bottom wall of the test section in order to trip the boundary layer. Thus, the separating boundary layer at the beginning of the cavity is turbulent. For most of the experiments described in this paper, the mean velocity above the cavity is $U_\infty = 1.20$ m/s, corresponding to Reynolds numbers of 4.0×10^4 based on cavity length. The mean pressure in the water-tunnel facility is well above the conditions that would cause occurrence of cavitation during the PIV measurements. The streamwise length of the cavity normalized by the momentum thickness of the boundary layer at the leading edge of the cavity, L/θ_0, is 127, sufficiently large for self-sustained shear layer oscillation. Based on Gharib[32] (1987) and Gharib & Roshko[33] (1987), the minimum L/θ_0 for such oscillation is about 80. The origin of the coordinate system used in this paper is placed at the leading edge of the cavity, with the x and y axes pointing downstream and upward, respectively. The instantaneous, ensemble averaged and fluctuating horizontal and vertical velocity components are denoted as u, v, $\overline{u}$, $\overline{v}$, u', and v', respectively.

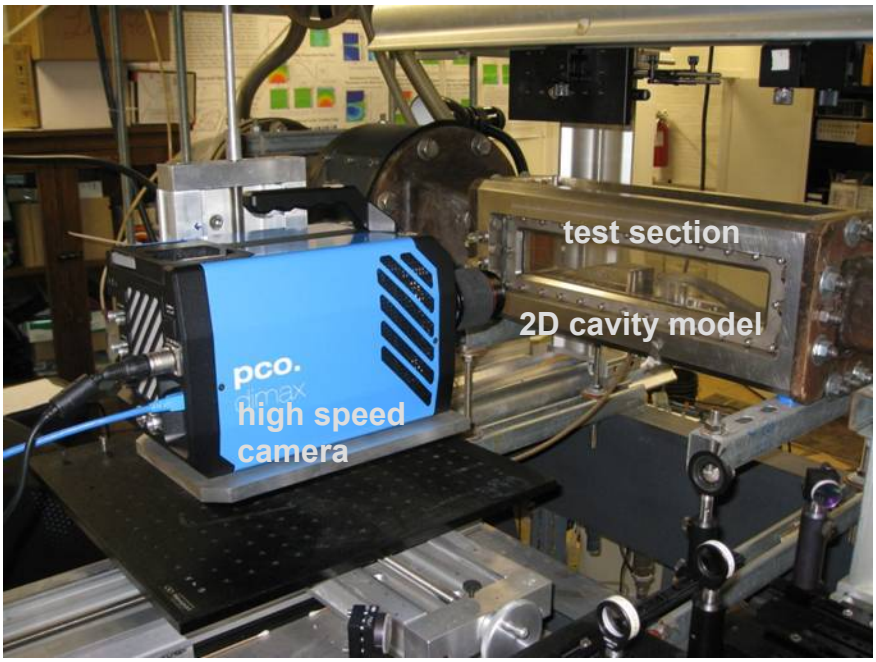

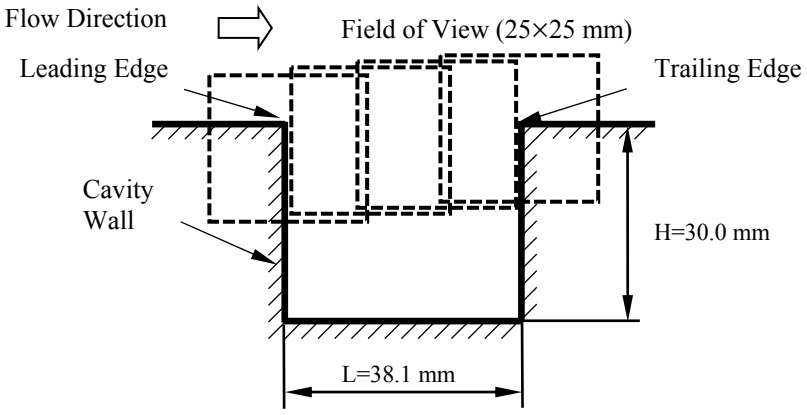

Figure 1. Experimental setup and cavity geometry.

To perform time-resolved, 2D PIV measurements, we utilize a Photonics DM60-527 Nd:YLF laser that has a maximum pulse rate of 10 kHz, and pulse width of 100 ns. The images are recorded at 4500 frames per second using

a PCO.dimax CMOS camera, at a resolution of 1008×1000 pixels, giving a Nyquist frequency of 2250 Hz for the velocity and 563 Hz for the material acceleration and pressure (see Section III for explanation). To synchronize the laser with the camera, we use a Quantum Composer model 9618 pulse generator. The selected temporal resolution is sufficient for resolving the Kolmogorov time scale, found to be 673 μs, based on curve fits to the spatial energy spectra to estimate the dissipation rate. The size of the field of view is 25×25 mm to maintain sufficient resolution, requiring us to record data in multiple adjacent sample areas, all aligned with the central plane of the cavity setup. With an appropriate concentration of seed particles, 8-12 μm diameter hollow glass spheres with specific gravity of 1.05-1.15, we are able to use an interrogation window size of 16×16 pixels, corresponding to 0.4×0.4 mm. This size is similar to the estimated Taylor transverse microscale of 0.5 mm, but is an order of magnitude larger than the Kolmogorov length scale of 26 μm. A 50% overlap between the interrogation windows gives a vector spacing of 0.2 mm. We use in-house developed software (Roth[34] 1998 and Roth & Katz[35] 2001) for calculating the velocity. A total of four sample areas with the same field-of-view size, but shifted horizontally with 50% overlap, are used to cover the flow field, from the boundary layer upstream of the leading corner to the flow over the trailing corner. The present analysis focuses on fields of view that cover the cavity trailing corners, where we have processed and analyzed eight datasets. Each set consists of 10,000 sequentially obtained instantaneous realizations over a period of 2.22 sec. Thus a total of 80,000 instantaneous realizations over 18 seconds were analyzed. These datasets cover only 30 flapping cycles for the trailing corner measurement station, which might affect the accuracy of the associated ensemble-averaged low-frequency components. We have also used velocity distributions obtained previously at a higher Reynolds number (3.4×10^5, Liu and Katz 2006, 2007, 2008) using a larger format camera, at the same spatial resolution (interrogation window of 0.4×0.4 mm), but at a much lower sampling frequency (2 Hz). In those measurements, the data consist of ensembles of 860 realizations that are not continuously time-resolved. The field of view is 50.8×50.8 mm covering the entire cavity, the vector spacing is 0.2 mm, and the free stream velocity is 10 m/s.

III. Analysis Procedures

The procedures for obtaining the velocity and the material acceleration, though still following the principle described in Liu & Katz[5] (2006), have been modified to take advantage of the time resolved data series. Analysis of each pair of consecutive images provides an instantaneous velocity distribution, and the entire set provides a time series $\vec{u}_1$, $\vec{u}_2$, $\vec{u}_3$, ... $\vec{u}_N$. Five consecutive images are used for calculating the acceleration. To calculate the velocity field at time t_i, we use

$$\vec{u}_i(\vec{x}_a,t_i)=\left(\vec{d}_{i,i+1}(\vec{x}_a,t_i)-\vec{d}_{i,i-1}(\vec{x}_a,t_i)\right)/(2\delta t) \qquad (1)$$

where $\vec{d}_{i,i+1}$ is the displacement of particles obtained from cross correlating the interrogation window in image *i* with that in image *i+1*. Thus, $\vec{u}_i(\vec{x}_a,t_i)$ is based on an average of $\vec{d}_{i,i+1}$ and $-\vec{d}_{i,i-1}$ of a group of particles located at $\vec{x}_a$ at time t_i. The in-plane projection of material acceleration is calculated using

$$\frac{D\vec{u}_i}{Dt}(\vec{x}_a,t_i)\approx\frac{\vec{u}_{i+1}\left(\vec{x}_a+\vec{d}_{i,i+1},t_{i+1}\right)-\vec{u}_{i-1}\left(\vec{x}_a+\vec{d}_{i,i-1},t_{i-1}\right)}{2\delta t} \qquad (2)$$

This approach estimates the material acceleration components from the difference between the velocity of the same group of particles at t_{i+1} and t_{i-1} as long as the majority of the particles remains within the light sheet. It is based on the assumption that the particles are displaced by the local velocity. Based on equations (1) and (2), a total of five consecutive images (*i*-2, *i*-1, *i*, *i*+1, *i*+2) are involved in the determination of the material acceleration, and subsequently, the pressure distribution. Thus the temporal resolution of the material acceleration and the pressure measurement is 888.9μs ($4\delta t$), giving rise to a corresponding Nyquist frequency of 563 Hz. Since the displacements involve fraction of the vector spacing, calculation of the acceleration involves bi-cubic interpolation (Liu and Katz 2006). As for the influence of the out-of-plane motion on the measurement accuracy, calculations based on four sets of data near the trailing corner show that $v_{rms}\partial u/\partial x|_{rms}$ (Note $w_{rms}\partial u/\partial z|_{rms}\approx v_{rms}\partial u/\partial x|_{rms}$) is not more than 14% of the measured rms fluctuations of $Du/Dt|_{rms}$ in the shear layer, and 5% outside of the shear layer. Detail discussions can be found in Liu and Katz[7] (2013).

The instantaneous pressure distribution is obtained by integrating the measured in-plane component of the material acceleration using *circular virtual boundary omni-directional integration* described in Liu and Katz[7] (2013) which is based on the algorithm introduced in Liu & Katz[5] (2006). For high Reynolds number flows away from the wall, the material acceleration is much larger in magnitude than the viscous terms, as confirmed by direct

calculations, and is balanced by the pressure gradients. The kernel of the pressure reconstruction procedure is the *Omni-Directional Integration*. By summing up the errors embedded in the measured pressure gradients from all directions, the omni-integration minimizes the influence of the errors propagated to the final pressure result, so as to achieve a reliable and accurate pressure measurement. A history about the evolution of the omni-directional integration algorithm can be found in Liu *et al.*[11] (2016), in which a novel *Rotating Parallel Ray omni-directional integration* method was introduced (yet not used in the analyses presented in this paper).

IV. Measurement Results on Pressure-Related Turbulence Statistics

A. Theory about Pressure-related Turbulence Terms

Since the time-averaged distributions of velocity, pressure, turbulence normal and shear stresses as well as spectral analysis for the shear flow over the cavity were presented in details in Liu and Katz[7] (2013), those quantities are not repeatedly presented in this paper. Instead, this paper focuses on the pressure-related turbulence statistics, including the pressure-velocity correlation, pressure diffusion and pressure-strain distributions around the trailing corner of the cavity, where those quantities vary most intensely due to the shear layer impingement on the cavity trailing wall.

In the Reynolds stress transport equation, the velocity-pressure gradient tensor

$$\Pi_{ij} = -\frac{1}{\rho}\overline{\left(u_i' \frac{\partial p'}{\partial x_j} + u_j' \frac{\partial p'}{\partial x_i} \right)} \qquad (3)$$

which can be further decomposed into pressure diffusion

$$-\frac{\partial T_{kij}^p}{\partial x_k} = -\frac{1}{\rho}\left(\frac{\partial \overline{u_j' p'}}{\partial x_i} + \frac{\partial \overline{u_i' p'}}{\partial x_j} \right) \qquad (4)$$

and pressure-strain tensors,

$$R_{ij} = \overline{\frac{p'}{\rho}\left(\frac{\partial u_i'}{\partial x_j} + \frac{\partial u_j'}{\partial x_i} \right)} \qquad (5)$$

i.e.,

$$\Pi_{ij} = R_{ij} - \frac{\partial T_{kij}^p}{\partial x_k} \qquad (6)$$

is critical for understanding and modeling turbulence (Pope[36] 2000; Girimaji[37] 2000). In the process of turbulence kinetic energy (TKE) transport, the pressure diffusion represents the mechanism due to pressure fluctuation for the redistribution of TKE from places where the energy is newly generated, to places where there is a lack of the new TKE, so as to help the turbulence field to become more homogeneous (Liu and Thomas[23], 2004). In contrast, the pressure-strain terms, as indicated by the equation

$$R_{11} + R_{22} + R_{33} = 0 \qquad (7)$$

are responsible for *redistribution of energy among components of the turbulence normal stresses*, i.e., *intermodal energy transfer among fluctuating components*, serving as the primary mechanism for the return-to-isotropy process (Pope[36] 2000) of the anisotropic turbulence commonly seen in turbulent shear flows, thus playing a major role in defining turbulence development. Two equation models like *k*-epsilon make no attempt to differentiate between the three fluctuating velocity components. Indeed if the transport equations for components of Reynolds normal stress $\overline{u'^2}$, $\overline{v'^2}$ and $\overline{w'^2}$ are summed, pressure-strain terms disappear altogether and so, do not appear in the turbulent kinetic energy transport equation. It is clear that *the intermodal energy transfer is a key to understanding the physics of turbulent shear flow*. It is based on the above observation and understanding that the pressure-related statistics are investigated in this study.

B. Pressure-Velocity Correlation

As shown in Equation (4), the pressure diffusion term involves the pressure-velocity correlation. Thus to investigate the behavior of the pressure diffusion, distributions of pressure-velocity correlation, including $\overline{p'u'}$ and $\overline{p'v'}$, are first examined and shown in Figures 2a and b. As can be seen in Figure 2a, in most of the shear layer, u' and p' are negatively correlated. This is in agreement with the distribution of the same quantity presented in a larger

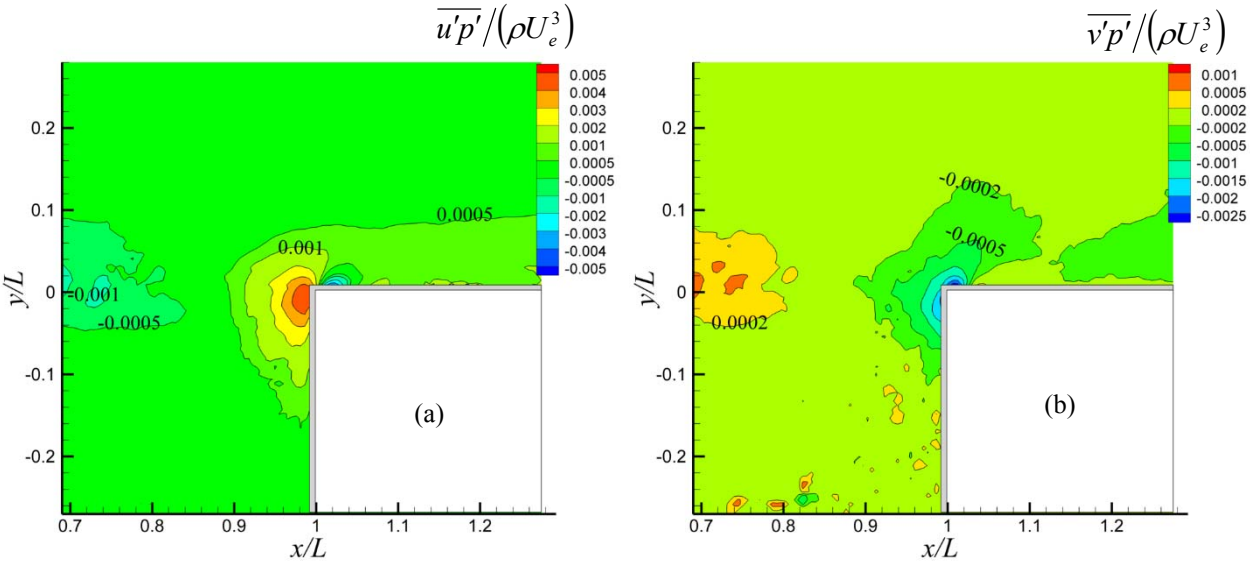

Figure 2. Distribution of pressure-velocity correlations: (a) correlation between the pressure and the streamwise velocity component; (b) correlation between the pressure and the lateral velocity component.

field of view for a 10m/s flow in the same cavity setup as shown in Figure 9 of Liu and Ktaz[38] (2007). This negative correlation, as discussed in Liu and Ktaz[38] (2007), implies that the pressure decreases as the instantaneous flow locally accelerates in the streamwise direction, and vice versa, i.e. an inertial "Bernoulli type" relation. Hooper and Musgrove[30] (1997), using a cobra (4-hole) probe, also report strong negative correlations between fluctuating pressure and streamwise velocity component in a developed pipe flow.

However, when the flow approaches the trailing edge of the cavity as shown in Figure 2a, due to the presence of the adverse pressure gradient, the negative-correlation of $\overline{p'u'}$ gradually decreases in magnitude and eventually changes its sign, creating a positive peak just upstream of the trailing edge. This trend must be associated with the adverse mean pressure gradients and stagnation-like conditions near the cavity forward corner. As the velocity, i.e., the momentum of the flow, increases in the impinging shear layer, the adverse pressure gradient also increases. Consequently, the pressure-velocity correlation becomes positive. This is again in agreement with the trend demonstrated in Liu and Katz[38] (2007).

As for the $\overline{p'v'}$ correlation shown in Figure 2b, p' and v' are positively correlated in most of the shear layer. To explain this trend, it is sufficient to note that essentially in all shear flows u' and v' are inherently negatively correlated (see Reynolds shear stress distribution in Figure 5f of Liu and Katz[7] 2013). A downward flow, i.e. negative v', brings high momentum fluid to the shear layer, i.e. a positive u'. This correlation also changes sign in front of the trailing edge. However, unlike the situation of $\overline{p'u'}$ shown in Figure 2a, where the correlation peak changes its sign from a positive one in front of the cavity trailing wall to a negative one immediately above the trailing corner, $\overline{p'v'}$ continuously maintains its negative correlation value in the area surrounding the trailing corner, as shown in Figure 2b. These complex behaviors of $\overline{p'u'}$ and $\overline{p'v'}$ around the impingement area are intriguing and apparently need further investigation in future so as to better understand the flow physics there.

C. Pressure Diffusion Distribution and Comparison with Turbulence Diffusion and Total Production Terms

Based on the distribution of the pressure velocity correlations, the corresponding pressure diffusion (also called *the gradient of the Reynolds stress flux due to fluctuating pressure*) of the Reynolds normal stresses of $\overline{u'^2}$ and $\overline{v'^2}$, can be evaluated and presented in Figures 3b and 4b, respectively. To gauge the distribution pattern and magnitude of the pressure diffusion terms, the corresponding turbulence diffusion of the Reynolds normal stresses are also shown in Figures 3a and 4a, respectively, together with the total turbulence production distribution shown in Figures 3c and 4c as an additional source for comparison. Clearly it can be seen that the turbulence diffusion of $\overline{u'^2}$ dominates in the shear layer. The three-layered distribution pattern of the turbulence diffusion of $\overline{u'^2}$ represents the transport of turbulence fluctuation energy away from the maximum mean shear location (the middle) of the shear

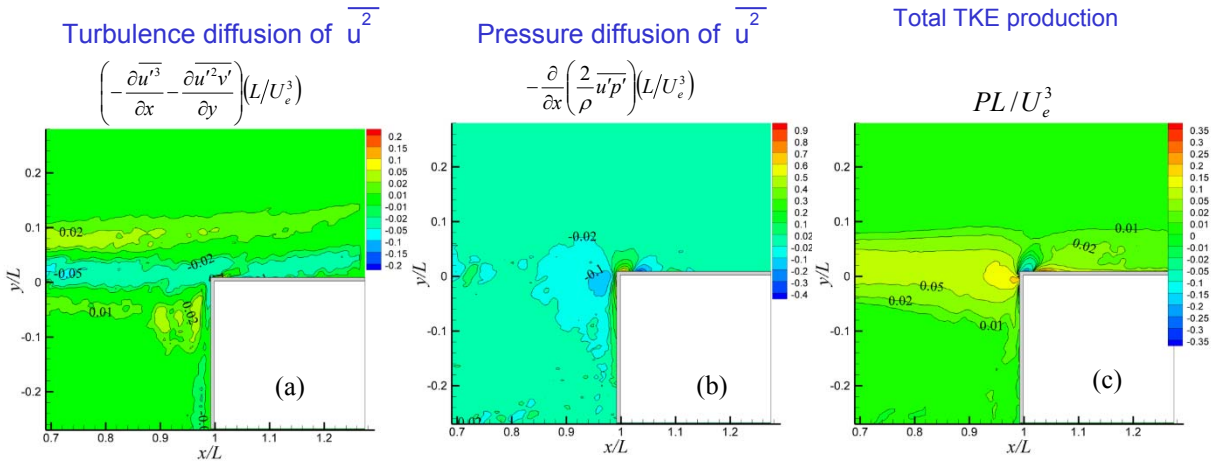

Figure 3. Comparison of (a) u-component turbulence diffusion, (b) u-component pressure diffusion and (c) total turbulence kinetic energy production terms in the turbulent shear layer impinging on the trailing corner of an open cavity.

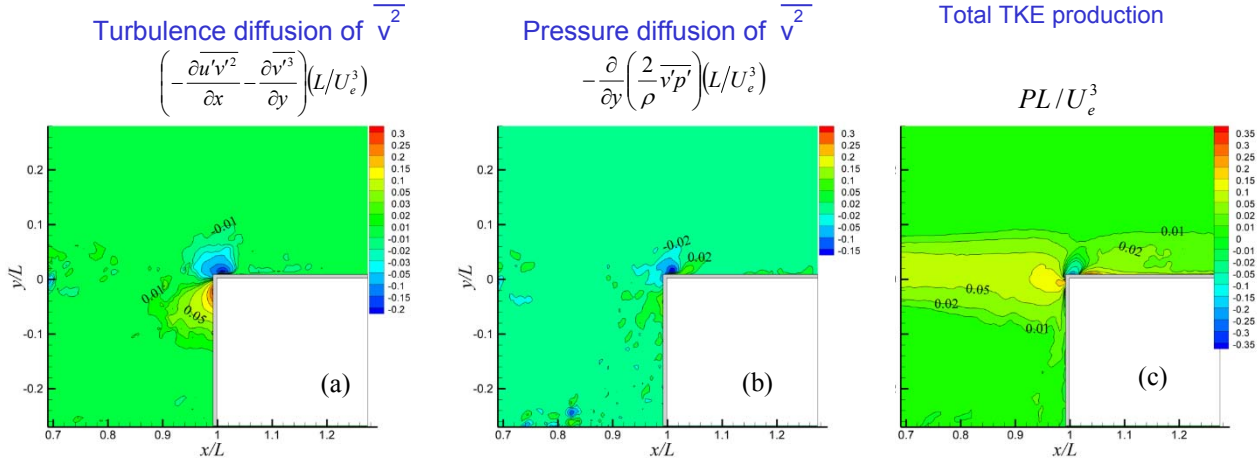

Figure 4. Comparison of (a) v-component turbulence diffusion, (b) v-component pressure diffusion and (c) total turbulence kinetic energy production terms in the turbulent shear layer impinging on the trailing corner of an open cavity.

layer, where turbulence shear production is most intense, to places near the upper and lower edges of the shear layer where there are lack of the newly generated fluctuation energy. This is consistent with the understanding of the turbulence diffusion mechanism as reported in Liu and Thomas[23] (2004) for TKE budget across the shear layers of a planar wake. In contrast, away from the corner, pressure diffusion is negligible. However, at places near the corner, pressure diffusion is significant, and its magnitude is on the same order of those for the turbulence diffusion and the total turbulence production terms, indicating that the pressure diffusion terms cannot be neglected near the trailing edge in RANS simulations of turbulent cavity flows. Moreover, comparing Figures 3b and c, it can be found that around the cavity trailing corner, the distribution patterns between the pressure diffusion of $\overline{u'^2}$ and the turbulence production terms are very similar, but with opposite signs. This similarity between the two distribution patterns is in agreement with the general understanding of the diffusion mechanism, i.e., newly generated turbulence is transported (diffused) to places lack of concentration of newly generated turbulence, such as the area on top of the trailing corner where the turbulence production is negative. The negative turbulence production, which tends to lead to the well-known "*relaminarization*" phenomenon[39] (Bourassa and Thomas, 2009), is a result of the local favorable pressure gradient. For this cavity flow, as shown in Figure 4f in Liu and Katz[7] (2013), a strong favorable pressure gradient region occurs around the tip of the cavity trailing corner. The low turbulence intensity (Figure 5 in Liu and Katz[7], 2013) as a result of the negative production on top of the cavity trailing-edge provides the foundation for a positive pressure diffusion of $\overline{u'^2}$ occurring there as shown in Figure 3b. Overall, the distribution patterns between

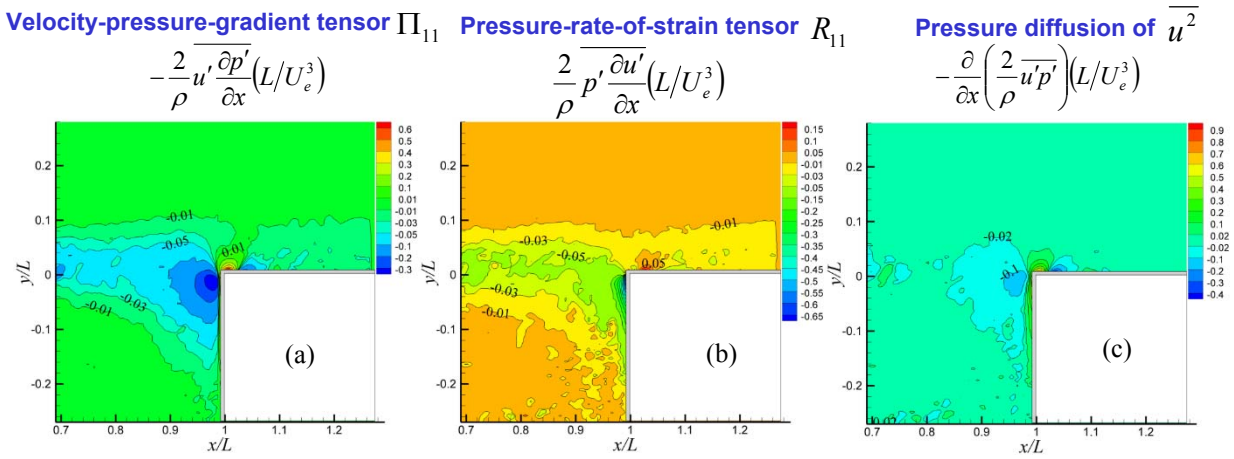

Figure 5. Comparison of u-component of (a) velocity-pressure-gradient tensor, (b) pressure-rate-of-strain tensor and (c) pressure diffusion terms measured in the turbulent shear layer impinging on the trailing corner of an open cavity.

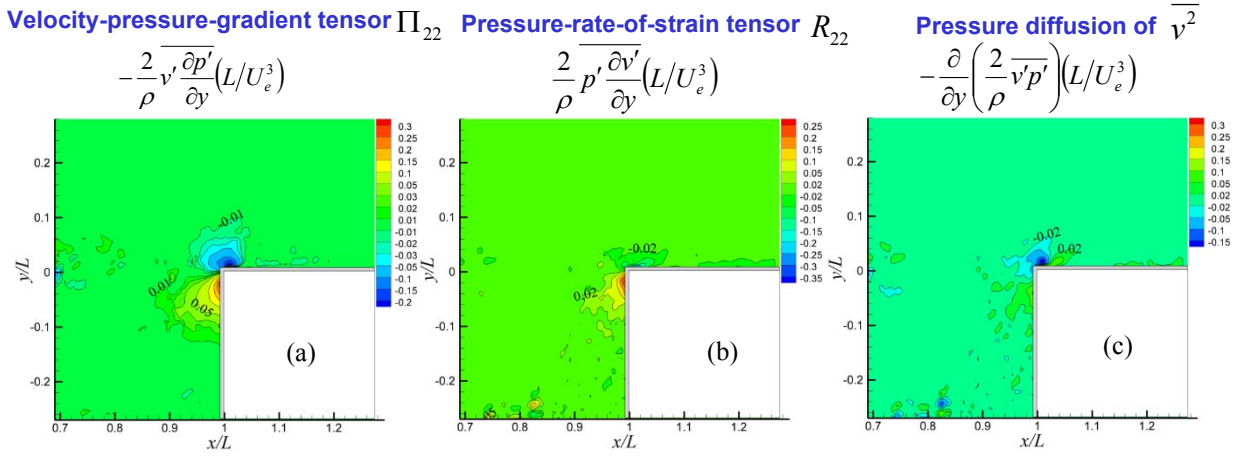

Figure 6. Comparison of v-component of (a) velocity-pressure-gradient tensor, (b) pressure-rate-of-strain tensor and (c) pressure diffusion terms measured in the turbulent shear layer impinging on the trailing corner of an open cavity.

the turbulence diffusion and the pressure diffusion are considerably different, implying that the conventional practice of modeling these transport terms together, typically as Laplacians of the turbulent kinetic energy (Pope[36] 2000; Chen and Jaw[40] 1998; Lumley[41] 1978; Fu[42] 1993; Schwarz and Bradshaw[43] 1994), may not be justifiable for this turbulent 2-D open cavity shear layer flow.

Peaks of the *v*-component pressure diffusion term are smaller in magnitude than those of the corresponding *u*-component pressure diffusion term. The values of these two types of terms are in opposite sign at corresponding locations surrounding the trailing corner of the cavity. Beyond the field of view shown in Figure 4, data in Liu and Katz[38] (2007) show that upstream around the mid-streamwise location of the shear layer, the *v*-component pressure diffusion is not negligible in comparison with the overall production rate. Clearly pressure-velocity correlations and subsequently the pressure diffusions have substantial impact on the dynamics of turbulence transport throughout the shear layer flow over the cavity.

D. Comparisons of Velocity-Pressure-Gradient, Pressure-Strain and Pressure Diffusion Terms

Figures 5 and 6 present the comparisons of the velocity-pressure-gradient, pressure-strain and pressure diffusion terms for the *u*- and *v*-components of Reynolds normal stress transport. To the best knowledge of the authors, this is the first time that these terms are measured for the shear layer flow over a cavity. All the terms shown in these two figures are calculated independently. The accuracy of the calculation is confirmed by plugging all measured terms into equation (6) and checking its validity. The common feature of all these three types of terms, for both the *u*- and

v-components, is that their peak magnitudes and the highest variations occur in the area surrounding the tip of the trailing corner of the cavity, where the highest and periodic pressure gradient variations occur (see Liu and Katz[7] 2013 for details about the pressure field characterization around the corner). In the shear layer, the *u*-component terms of the velocity-pressure-gradient Π_{11} and the pressure-strain R_{11} have dominant values in comparison with their counterparts in the *v*-component terms, which seem negligible.

It is interesting to note that the pressure-strain term R_{11} keeps a strong negative value (~ -0.05) throughout the shear layer. This value is strengthened significantly (~ -0.65) at the impingement point on the trailing wall of the cavity. In contrast, the magnitude of the pressure-strain term R_{22} appears with a quite weak positive value in the shear layer. This is consistent with the magnitudes of the Reynolds normal stress $\overline{u'^2}$ and $\overline{v'^2}$ distributions as shown in Figure 5 in Liu and Katz[7] (2013), where clearly the streamwise *u*-component fluctuation is the dominant fluctuating velocity component, thus rending its negative value in R_{11}, i.e., implying the loss of energy from $\overline{u'^2}$ to other components. Based on the above discussion, it seems that at least in the shear layer, major loss in the *u*-component fluctuation energy would be mainly absorbed by the spanwise *w*-component. Thus 3D data in future experiment may be needed to bring this conjecture into a closure.

It is also interesting to note that close to the impingement point, the amount of share of the intermodal fluctuation energy transfer that the *v*-component absorbs significantly increases up to a magnitude of ~0.25, as indicated from the R_{22} distribution plot. Thus, considering the ~ -0.65 loss of the fluctuation energy of the *u*-component at that place, the amount the fluctuation energy that the *w*-component absorbs at that location can be inferred as 0.40 according to equation (7).

In contrast, the intermodal fluctuation energy transfer completely changes its scheme shortly downstream of the trailing edge above the trailing corner, where R_{11} takes a positive value of ~ 0.15, and R_{22} a negative value of ~ -0.35, meaning that the *v*-component fluctuation is losing energy and the *u*-component fluctuation is gaining energy. These variations are in agreement with the local $\overline{u'^2}$ and $\overline{v'^2}$ variations on top of the trailing corner as shown clearly in the insets of Figure 5(b) and (d) in Liu and Katz[7] (2013), where $\overline{u'^2}$ is gaining fluctuation energy along the streamwise direction while $\overline{v'^2}$ at the same time is losing energy in the same region on top of the trailing corner. This is a good example demonstrating the key role that the pressure-strain term plays in redistribution of energy among components of the turbulence normal stresses, i.e., the intermodal energy transfer among fluctuating components.

The complicated intermodal energy transfer process described above clearly shows the challenge (and perhaps opportunities) that turbulence modeling for Reynolds stress transport faces in the situation of turbulent shear layer flow over an open cavity in particular, and separation and reattachment flow in general.

V. Conclusions and Future Work

Pressure-velocity correlation, pressure diffusion, pressure-rate-of-strain and velocity-pressure-gradient tensors have been measured in a 2D open cavity shear flow at a Reynolds number of 40,000 based on the cavity length. To the best of our knowledge, this is the first time that these important terms are experimentally measured in a cavity shear layer flow. The measurement results lead to the following interesting conclusions:

- In most of the shear layer, u' and p' are negatively correlated. However, as the flow approaches the trailing edge of the cavity, due to the presence of the adverse pressure gradient, the negative-correlation of $\overline{p'u'}$ gradually decreases in magnitude, and eventually changes its sign, creating a positive peak just upstream of the trailing edge. As for the $\overline{p'v'}$ correlation, p' and v' are positively correlated in most of the shear layer. However, unlike $\overline{p'u'}$, which changes its sign from a positive one in front of the cavity trailing wall to a negative one immediately above the trailing corner, $\overline{p'v'}$ continuously maintains its negative correlation value in the area surrounding the cavity trailing corner.
- The turbulence diffusion of $\overline{u'^2}$ dominates in the shear layer. Away from the corner, pressure diffusion is negligible. However, close to the corner, pressure diffusion is significant, and its magnitude is on the same order as those of the turbulence diffusion and the total turbulence production, indicating that the pressure diffusion terms cannot be neglected near the cavity trailing edge in RANS simulations.
- The distribution patterns of the turbulence diffusion and the pressure diffusion are considerably different. Thus the conventional practice of modeling the transport terms all together as Laplacians of the turbulent kinetic energy is not justifiable at least for the turbulent 2-D open cavity flow.

- The *u*- and the *v*-component pressure diffusion terms have opposite signs at corresponding locations surrounding the trailing corner of the cavity, where the peaks of the *v*-component pressure diffusion are smaller in magnitude than those of the *u*-component counterparts.
- In the shear layer, the *u*-component velocity-pressure-gradient tensor Π_{11} and the pressure-strain R_{11} have dominant values in comparison with their *v*-component counterparts. The pressure-strain term R_{11} keeps a strong negative value throughout the shear layer and strengthens it significantly at the impingement point on the trailing wall of the cavity. In contrast, the pressure-strain term R_{22} has a quite weak positive value in the shear layer. This is consistent with the magnitudes of the Reynolds normal stresses $\overline{u'^2}$ and $\overline{v'^2}$ distributions in the flow field.
- Close to the impingement point, the amount of the intermodal fluctuation energy transfer that the *v*-component fluctuation receives significantly increases to about 1/3 of the energy loss from the *u*-component fluctuation.
- The intermodal fluctuation energy transfer completely changes its scheme on top of the trailing corner, where R_{11} takes a positive value and R_{22} a negative one, indicating that the *u*-component fluctuation is gaining while the *v*-component fluctuation is losing energy. This is consistent with the local Reynolds normal stress $\overline{u'^2}$ and $\overline{v'^2}$ variations according to data published before on the same experiment.

The complicated intermodal energy transfer process described above clearly shows the challenge (and perhaps opportunities) that turbulence modeling for Reynolds stress transport faces in the situation of turbulent shear layer flow over an open cavity in particular, and separation and reattachment flow in general. Clearly the pressure diffusion and the pressure-strain distributions have substantial impact on the dynamics of turbulence transport throughout the shear layer. The complex behaviors of the pressure-related turbulence transport terms around the impingement area are intriguing and apparently need further investigation in future so as to better understand the flow physics there.

Acknowledgments

The research was sponsored in part by the Office of Naval Research (Ki-Han Kim and Debbie Nalchajian are the Program Officers), and in part by National Science Foundation grant No. 0932941 (H. Henning Winter is the program Director). The financial support from the UGP program of the San Diego State University is also gratefully acknowledged.

References

[1]Oden, J.T. (chair), 2006, "Simulation-based engineering science – Revolutionizing engineering science through simulation", National Science Foundation.

[2]Slotnick J., Khodadoust, A., Alonso, J., Darmofal, D., Gropp, W., Lurie, E. and Mavriplis, D., 2014, "CFD vision 2030 study: A path to revolutionary computational aerosciences". NASA/CR-2014-218178.

[3]Wilcox, D.C, 2006, "Turbulence modeling for CFD", DCW Industries, 3rd Edition.

[4]Liu, X. and Katz, J., 2003, "Measurements of Pressure Distribution by Integrating the Material Acceleration", Cav03-GS-14-001, *Proc. of the 5th International Symposium on Cavitation (Cav2003)*, Osaka, Japan, Nov. 1-4, 2003.

[5]Liu, X. and Katz, J., 2006, "Instantaneous Pressure and Material Acceleration Measurements using a Four Exposure PIV System," *Exp. Fluids*, Vol. 41, No. 2, August 2006, pp227-240.

[6]Liu, X. and Katz, J., 2008, "Cavitation Phenomena Occurring due to Interaction of Shear Layer Vortices with the Trailing Corner of a 2D Open Cavity," *Physics of Fluids*, Vol. 20, No. 4, April 2008, 041702, DOI:10.1063/1.2897320.

[7]Liu, X. and Katz, J., 2013, "Vortex-Corner Interactions in a Cavity Shear Layer Elucidated by Time Resolved Measurements of the Pressure Field," *J. Fluid Mech.*, Vol. 728, August 2013, pp 417-457. DOI: 10.1017/jfm.2013.275.

[8]Van Oudheusden BW, 2008, "Principles and application of velocimetry-based planar pressure imaging in compressible flows with shocks", *Exp. Fluids*, 45, 657–674.

[9]Ragni, D., Ashok, A., Van Oudheusden, B. W. and Scarano, F., 2009, "Surface Pressure and Determination of a Transonic Aerofoil Based on Particle Image Velocimetry," *Meas. Sci. Technol.*, Vol. 20, No. 7, July 2009, 074005.

[10]Joshi, P., Liu, X. and Katz, J., 2014, "Effect of mean and fluctuating pressure gradients on boundary layer turbulence", *J. Fluid Mech.*, Vol. 748, June 2014, pp. 36–84. DOI:10.1017/jfm.2014.147.

[11]Liu, X, Moreto, J. R. and Siddle-Mitchel, S., 2016, "Instantaneous Pressure Reconstruction from Measured Pressure Gradient using Rotating Parallel Ray Method", AIAA-2016-1049, 54th AIAA Aerospace Sciences Meeting, AIAA SciTech, Jan. 2016, doi: 10.2514/6.2016-1049.

[12]De Kat, R. and Van Oudheusden, B. W., 2010, "Instantaneous planar pressure from PIV: analytic and experimental test-cases". In *15th International Symposium on Applications of Laser Techniques to Fluid Mechanics*, Lisbon, Portugal, July 5-8, 2010.

[13]De Kat, R. and Van Oudheusden, B. W. 2012, "Instantaneous planar pressure determination from PIV in turbulent flow", *Exp Fluids* Vol. 52, No. 5, pp. 1089–1106, May 2012.

[14]Violato, D., Moore, P. and Scarano, F., 2011, "Lagrangian and Eulerian Pressure Field Evaluation of Rod-Airfoil Flow from Time-Resolved Tomographic PIV", *Exp. Fluids*., Vol.50, No. 4, April 2011, pp. 1057–1070.

[15]Auteri, F., Carina, M., Zagaglia, D., Montagnon, D., Libertine, G., Mars, C. B. and Zanetti, A., 2015, "A Novel Approach for Reconstructing Pressure from PIV Velocity Measurements," *Exp Fluids*, Vol, 56 , No.45, February 2015, DOI 10.1007/s00348-015-1912-z.

[16]Charonko, J. J., King, C. V., Smith, B. L. and Vlachos, P. P., 2010, "Assessment of Pressure Field Calculations from Particle Image Velocimetry Measurements," *Meas. Sci. Technol.*, Vol. 21, No.10, October 2010, 105401.

[17]Van Oudheusden, B. W., 2013, "PIV-based pressure measurement," *Meas. Sci. Technol.* Vol. 24, No.3, March 2013, 032001.

[18]Jeon, Y.J., Chatellier, L., Beaudoin, A., and David, L., 2015, "Least-square reconstruction of instantaneous pressure field around a body based on a directly acquired material acceleration in time-resolved PIV", *11th International Symposium on Particle Image Velocimetry – PIV15*, Santa Barbara, California, September 14-16, 2015.

[19]Liu, X. and Katz, J., 2007, "Measurement of pressure-rate-of-strain, pressure diffusion and velocity-pressure-gradient tensors in a cavity shear layer by integrating the material acceleration", APS Division of Fluid Dynamics, November 18-20, 2007, abstract #NQ.010, Bulletin of the American Physical Society, Vol. 52: p295.

[20]Liu, X. and Katz, J., 2008, "Measurement of pressure-rate-of-strain, pressure diffusion and velocity-pressure-gradient tensors around an open cavity trailing corner", APS Division of Fluid Dynamics, November 23-25, 2008, abstract #HC.004, Bulletin of the American Physical Society, Vol. 53 , No.15, p 177.

[21]Liu, X. and Katz, J., 2014, "Pressure rate of strain, pressure diffusion and velocity pressure gradient tensor measurements in a cavity shear layer flow", APS Division of Fluid Dynamics, November 23-25,2014, abstract #D25.008, Bulletin of the American Physical Society, Vol. 59, No.20, p 137.

[22]Kawata T., Obi, S., 2014, "Velocity–pressure correlation measurement based on planar PIV and miniature static pressure probes", *Exp. Fluids*, 55: 1776. doi:10.1007/s00348-014-1776-7.

[23]Liu, X. and Thomas, F.O., 2004, "Measurement of the turbulent kinetic energy budget of a planar wake flow in pressure gradients", *Experiments in Fluids*, 37:469-482.

[24]Gutmark, E. and Wygnanski, I., 1976, "The planar turbulent jet," *J. Fluid Mech.*, 73:465-495.

[25]Wygnanski, I. and Fiedler H., 1969, "Some measurements in self-preserving jet", J. Fluid Mech., 38:577-612.

[26]Kawata, T., Naka, Y. and Obi, S., 2014, "Simultaneous measurement of fluctuating velocity and pressure in the near wake of a circular cylinder", *Exp. Fluids*, 55:1731. Doi: 10.1007/s00348-014-1731-7.

[27]Terashima, O., Sakai, Y. and Nagata, K., 2012, "Simultaneous measurement of velocity and pressure in a plane jet", *Exp Fluids*, 53:1149–1164. doi 10.1007/s00348-012-1351-z.

[28]Naka Y., Obi S., 2009, "Velocity-pressure correlation measurements in complex free shear flows", *Int J Heat Fluid Flow*, Vol. 30, No. 3, June 2009, pp 411–420.

[29]Naka Y., Omori T., Obi S., Masuda S., 2006, "Simultaneous measurement of fluctuating velocity and pressure in a turbulent mixing layer", *Int J Heat Fluid Flow*, 27:737–746.

[30]Hooper, J.D. and Musgrove, A.R., 1997, "Reynolds stress, mean velocity, and dynamic static pressure measurement by a four-hole pressure probe", *Experimental Thermal and Fluid Science*, Vol. 15, No. 4, November 1997, pp 375-383.

[31]Gopalan, S. and Katz, J., 2000, "Flow structure and modelling issues in the closure region of attached cavitation", *Phys. Fluids* 12, 895–911.

[32]Gharib, M., 1987, "Response of the cavity shear layer oscillations to external forcing". *AIAA J.* 25, 1, 43-47.

[33]Gharib, M. and Roshko A., 1987, "The effect of flow oscillations on cavity drag". *J. Fluid Mech.* 177, 501-530.

[34]Roth, G.I., 1998, "Developments in particle image velocimetry (PIV) and their application to the measurement of the flow structure and turbulence within a ship bow wave". PhD dissertation, Johns Hopkins University, Baltimore, MD.

[35]Roth, G.I. and Katz. J. 2001, "Five techniques for increasing the speed and accuracy of PIV interrogation". Meas. Sci. Technol. 12, 238–245.

[36]Pope S.B., 2000, *Turbulent flows*, Cambridge Univ. press.

[37]Girimaji, S.S., 2000, "Pressure-strain correlation modeling of complex turbulent flows", *J. Fluid Mech.*, 422: 91-123.

[38]Liu, X. and Katz, J., 2007, "A comparison of cavitation inception index measurements to the spatial pressure distribution within a 2D cavity shear flow", FEDSM2007-37090. In 5th Joint ASME/JSME Fluids Engineering Conference, San Diego, California.

[39]Bourassa, C. and Thomas, F.O., 2009, "An experimental investigation of a highly accelerated turbulent boundary layer". *J. Fluid Mech.* 634, 359–404.

[40]Chen, C.-J. and Jaw, S.-Y., 1998, *Fundamentals of turbulence modeling*, Taylor and Francis.

[41]Lumley, J.L., 1978, "Computational modeling of turbulent flows", *Advances in Applied Mechanics*, 18: 123-176.

[42]Fu, S., 1993, "Modeling of the pressure-velocity correlation in turbulence diffusion", *Computers Fluids*, 22:199-205.

[43]Schwarz, W.R. and Bradshaw, P., 1994, "Term-by-term tests of stress-transport turbulence models in a three-dimensional boundary layer," *Phys. Fluids*, 6: 986-998.